SciForschen
Open HUB for Scientific Research

ISSN: 2470-3206

International Journal of Nanomedicine and Nanosurgery

Research Article | Volume: 2.2 | Open Access

Development of Magnetic Nanocarriers based on Thermosensitive Liposomes and their Visualization using Magnetic Particle Imaging

Shuki MARUYAMA, Kazuki SHIMADA, Kohei ENMEIJI and Kenya MURASE*

Department of Medical Physics and Engineering, Division of Medical Technology and Science, Faculty of Health Science, Graduate School of Medicine, Osaka University, Suita, Osaka, Japan

***Corresponding author:** Kenya Murase, Ph.D, Department of Medical Physics and Engineering, Division of Medical Technology and Science, Faculty of Health Science, Graduate School of Medicine, Osaka University 1-7 Yamadaoka, Suita, Osaka 565-0871, Japan, Tel: 81-6-6879-2571; Fax: +81-6-6879-2571; **E-mail:** murase@sahs.med.osaka-u.ac.jp

Received date: 23 Feb 2016; **Accepted date:** 31 Mar 2016; **Published date:** 04 Apr 2016.

Citation: Maruyama S, Shimada K, Enmeiji K, Murase K (2016) Development of Magnetic Nanocarriers based on Thermosensitive Liposomes and their Visualization using Magnetic Particle Imaging. Int J Nanomed Nanosurg 2(2): doi http://dx.doi.org/10.16966/2470-3206.111

Abstract

Purpose: The purpose of this study was to develop magnetic nanocarriers by encapsulating magnetic nanoparticles (MNPs) and calcein or doxorubicin (DOX) into thermosensitive liposomes (TSLs), and to investigate the feasibility of visualizing them using magnetic particle imaging (MPI) and the therapeutic effect of chemotherapy using the DOX release induced by magnetic hyperthermia (MH) using tumor-bearing mice.

Materials and methods: First, the TSLs were prepared using a lipid mixture composed of 1,2-dipalmitoyl-sn-glycero-3-phosphocholine (DPPC) and polyoxyethylene (20) stearyl ether (Brij78®) at a molar ratio of 96 : 4. Second, we encapsulated both MNPs and calcein into the TSLs and imaged them using our MPI scanner. The net iron concentration in the magnetic TSLs was measured by the potassium thiocyanate method. We also heated the magnetic TSLs using our system for MH. Finally, we developed TSLs encapsulating both MNPs and DOX (DOX-TSLs) and performed animal experiments. After the DOX-TSLs were administered directly into the tumors of tumor-bearing mice, the mice were scanned using our MPI scanner and then underwent MH.

Results: The calcein release from the TSLs steeply increased at about 38-40°C and plateaued thereafter, whereas it was almost zero at 27-36°C. The magnetic TSLs were successfully visualized using our MPI scanner. The average MPI pixel value showed significant correlations with the net iron concentration in the magnetic TSLs and the temperature rise induced by MH. When the DOX-TSLs were injected into tumors and MH was applied, the relative tumor volume growth was significantly lower than that in the case when MH was not applied, suggesting a therapeutic effect of the chemotherapy using the DOX release induced by MH.

Conclusion: Our results suggest that our magnetic TSLs are useful as drug delivery nanocarriers in nanomedicine. Our results also suggest that MPI is useful for enhancing the effectiveness of chemotherapy based on the drug release from TSLs, because MPI can visualize the magnetic TSLs in positive contrast allowing us to estimate the iron concentration in the magnetic TSLs for predicting the drug release induced by MH.

Keywords: Thermosensitive liposomes; Magnetic particle imaging; Magnetic hyperthermia treatment; Magnetic nanoparticles; Doxorubicin

Introduction

The use of nanoparticles in diagnosis and therapy for cancer is progressively growing, and may be one of the most important developments in drug delivery systems. Liposomes are highly biocompatible and biodegradable nanosized particles and can enclose hydrophilic drugs in the inner aqueous cavity [1,2]. Liposome-based anticancer chemotherapy has attracted much attention due to its advantage of reducing cytotoxicity in healthy tissues by encapsulating drugs. Hence, several multi-functional liposome formulations have been investigated with a view to clinical use in recent years. For instance, polyethylene glycol (PEG)-coated long-circulating liposomes encapsulating doxorubicin (DOX) have already been approved in the clinical setting [3,4]. Yatvin et al. [5] developed thermosensitive liposomes (TSLs) entrapping anticancer drugs for the first time in 1978. TSLs are one of the most promising tools for cancer therapy when used in combination with local hyperthermia. TSLs made with 1, 2-dipalmitoyl-sn-glycero-3-phosphocholine (DPPC) are designed to release encapsulated drugs at the melting phase transition temperature of the lipid bilayer [1]. Recently, much effort has been put into the development of new TSL formulations. In 2011, Tagami et al. [6,7] reported a novel TSL formulation composing of DPPC and polyoxyethylene (20) stearyl ether (Brij78®) at a molar ratio of 96 : 4 (hyperthermia-activated-cytotoxic (HaT)-liposome) and that the HaT-liposomes encapsulating gadolinium-diethylenetriaminepentaacetic acid (Gd-DTPA) could be used in hyperthermia combined with drug delivery under monitoring by magnetic resonance imaging (MRI).

Hyperthermia is one approach to cancer therapy. However, there is a technical difficulty in local heating to the hyperthermic condition without damaging surrounding normal tissues [8,9]. Hyperthermia using magnetic nanoparticles (MNPs) (magnetic hyperthermia: MH) has gained much attention in recent years because it solves this problem. MNPs have been widely used in nanomedicine for their high versatility. MNPs generate heat when exposed to an alternating magnetic field (AMF) as a result of magnetic hysteresis and/or relaxational losses (Brownian and Néel relaxations) [10,11]; this results in heating of the tissue in which MNPs have accumulated [12].

In addition, MNPs based on superparamagnetic iron oxide (maghemite or magnetite) have been used as contrast agents for MRI. The use of these agents enhances negative contrast on transverse relaxation time (T2*)-

weighted images due to shortening of T2*. Béalle et al. [13] prepared magnetic liposomes named Ultra Magnetic Liposomes, which were suitable for systemic delivery and characterized by an outstanding loading potential of MNPs through the incorporation of a high amount of MNPs in the aqueous core of the vesicle. The high encapsulation of MNPs into liposomes allows for efficient MRI detection, magnetic targeting, and heating of the sites of interest while minimizing the injected dose [13].

Recently, a new imaging method called magnetic particle imaging (MPI) has been introduced [14]. MPI allows imaging of the spatial distribution of MNPs with high sensitivity, spatial resolution, and imaging speed [14]. MPI uses the nonlinear response of MNPs to detect their presence in an AMF, which is referred to here as the drive magnetic field. Spatial encoding is accomplished by saturating the MNPs over most of the imaged region using a static magnetic field (selection magnetic field), except in the vicinity of a special position called the field-free point [14] or field-free line [15]. We have developed a system for MPI with a field-free-line encoding scheme, in which the field-free line is generated using two opposing neodymium magnets, and transverse images are reconstructed from the third-harmonic signals received by a gradiometer coil using the maximum likelihood-expectation maximization (ML-EM) algorithm [16,17].

TSLs encapsulating both MNPs and anticancer drugs have the potential to be applied not only for diagnosis using MPI as a contrast agent but also to chemotherapy using the drug release induced by MH. The purpose of this study was to develop TSLs encapsulating MNPs and calcein or DOX and to investigate the feasibility of visualizing them using MPI *in vitro* and *in vivo* and the therapeutic effect of chemotherapy using the DOX release induced by MH *in vivo*.

Materials and Methods

Materials

DPPC and Brij78® were purchased from Wako Pure Chemical Industries, Ltd. (Osaka, Japan). Bis [N,N-bis (carboxymethyl) aminomethyl] fluorescein (calcein) was manufactured by Dojindo Co., Ltd. (Kumamoto, Japan) and purchased from Wako Pure Chemical Industries, Ltd. (Osaka, Japan). Potassium thiocyanate and ammonium sulphate were purchased from Wako Pure Chemical Industries, Ltd. (Osaka, Japan). Magnetic fluid M-300 (magnetite, Fe_3O_4) was purchased from Sigma Hi-Chemical Inc. (Kanagawa, Japan). Phosphate buffered saline (PBS) (NaCl 137 mM, KCl 2.7 mM, Na_2HPO_4 10 mM and KH_2PO_4 2 mM, pH 7.4) was purchased from Wako Pure Chemical Industries, Ltd. (Osaka, Japan). DOX hydrochloride was purchased from Kyowa Hakko Kirin Co., Ltd. (Tokyo, Japan).

Preparation of TSLs encapsulating calcein: The TSLs encapsulating calcein were prepared by thin film and hydration methods [18]. First, 20 mg/mL of a lipid mixture composed of DPPC and Brij78® at a molar ratio of 96:4 was dissolved in ethanol in a round-bottom flask. The solvent was removed by a rotary evaporator and desiccated for 24 h. The lipid mixture was hydrated at 65°C by adding a PBS solution of calcein (63 mM) with the pH adjusted to 7.4. The suspension obtained was sonicated for 5 min, and the sonication was repeated four times with intervals of 1 min. Unencapsulated calcein was removed by gel chromatography using Sepharose gel in a CL-2B column (2 cm in diameter and 50 cm in length) (GE Healthcare Japan Co., Ltd., Tokyo, Japan) with a flow rate of 1 mL/min, and PBS was used as the elution solution.

Measurement of calcein release: The calcein release from the calcein-loaded TSLs was measured using the self-quenching phenomenon of calcein fluorescence [18]. Briefly, a 60 µL suspension of the liposome solution containing calcein was added to 600 µL PBS in a micro tube. The samples obtained from the suspension were incubated for 20 min at each temperature starting at 27°C and increasing to 34, 36, 38, 40, 42, 44°C using a block incubator (BI-516S, ASTEC Co., Ltd., Fukuoka, Japan). Twenty µL of each sample was diluted by adding 2 mL of PBS, and the sample was placed in a 96-well plate for the measurement of fluorescence intensity. The fluorescence intensity was measured using a plate reader (F-7000, Hitachi Co., Tokyo, Japan) at an excitation wavelength of 485 nm and an emission wavelength of 520 nm. To measure the maximal release of calcein, 60 µL of the suspension was added to 600 µL PBS containing 1% Triton X-100 (Wako Pure Chemical Industries, Ltd., Osaka, Japan) in a weight ratio (6 µL) and incubated for 20 min at 50°C to destroy the liposomal membrane. The percentage of the calcein release from the calcein-loaded TSLs was calculated as in Equation 1:

$$\text{Release}(\%) = \frac{F_a - F_b}{F_t - F_b} \times 100 \quad \text{.....(1)}$$

Where F_b and F_a denote the fluorescence intensities of the liposome suspension before incubation and after 20 min incubation at a given temperature, respectively, and F_t is the fluorescence intensity of the sample treated by Triton X-100. The relationship between the temperature and calcein release was fitted to a sigmoid function given by Equation 2 using the non-linear least-squares method [19].

$$f(x) = \frac{a}{1 + e^{-b(x-c)}} \quad \text{.....(2)}$$

Where a, b, and c are constants.

Preparation of TSLs loading DOX: The TSLs loading DOX were prepared according to the procedure described above with some minor modifications [6,7]. First, 20 mg/mL of the lipid mixture composed of DPPC and Brij78® at a molar ratio of 96:4 was dissolved in ethanol in a round-bottom flask. The solvent was removed by a rotary evaporator and desiccated for 24 h. The lipid mixture was hydrated at 65°C by adding 280 mM ammonium sulphate (pH 4-4.5). The suspension obtained was sonicated for 5 min, and the sonication was repeated four times with intervals of 1 min. After the TSL solution was cooled to room temperature, DOX was encapsulated into the TSLs by the pH gradient method [6,7]; the exterior solution of the liposome suspension was replaced by PBS via dialysis for 3 h against three exchanges of 500 × volumes of PBS. The liposome suspension and DOX were mixed at a DOX to lipid ratio of 0.05 (w/w) and the mixture was incubated at 37°C for 90 min. The unencapsulated DOX was removed by gel chromatography as described above for calcein.

Measurement of DOX release: The DOX release was also measured using the self-quenching phenomenon of DOX fluorescence [18]. In brief, 200 µL suspension of the liposome solution containing DOX was added to 200 µL PBS in a micro tube. The samples obtained from the suspension were incubated for 20 min at each temperature starting at 27°C and increasing to 34, 36, 38, 40, 42, 44°C using a block incubator (BI-516S, ASTEC Co., Ltd., Fukuoka, Japan), and then the sample was placed in a 96-well plate for the measurement of fluorescence intensity. The fluorescence intensity was measured using a plate reader (F-7000, Hitachi Co., Tokyo, Japan) at an excitation wavelength of 485 nm and an emission wavelength of 590 nm. The percentage of the DOX release from the TSLs was calculated from Equation 1. The relationship between the temperature and DOX release was also fitted using a sigmoid function as described above.

Phantom experiments

System for MPI: The details of our MPI system are described in our previous papers [16,17,20-23]. In brief, the field-free line was generated by two opposing neodymium magnets. The drive magnetic field was generated using an excitation coil (solenoid coil 100 mm in length, 80

mm in inner diameter, and 110 mm in outer diameter). AC power was supplied to the excitation coil by a programmable power supply (EC1000S, NF Co., Kanagawa, Japan), and was controlled using a sinusoidal wave generated by a digital function generator (DF1906, NF Co., Kanagawa, Japan). The frequency of the drive magnetic field was 400 Hz, and the peak-to-peak strength of the drive magnetic field was 20 mT. The MNP-generated signal was detected by a gradiometer coil (50 mm in length, 35 mm in inner diameter, and 40 mm in outer diameter) and the third-harmonic signal was extracted using a preamplifier (T-AMP03HC, Turtle Industry Co., Ibaragi, Japan) and a lock-in amplifier (LI5640, NF Co., Kanagawa, Japan). The output of the lock-in amplifier was converted to digital data using a personal computer connected to a multifunction data acquisition device with a universal serial bus port (USB-6212, National Instruments Co., TX, USA). The sampling time was taken as 10 ms. When measuring signals using the gradiometer coil, the sample was placed 12.5 mm (i.e., one quarter of the coil length) from the center of the gradiometer coil and the coil, including the sample, was moved such that the center of the sample coincided with the position of the field-free line. The selection magnetic field was generated by two opposing neodymium magnets (Neomax Engineering Co., Gunma, Japan). The field-free line can be generated at the center of the two neodymium magnets. To acquire projection data for image reconstruction, both the sample and the receiving coil were automatically rotated around the z-axis over 180° in steps of 5° and translated in the x-direction from −16 mm to 16 mm in steps of 1 mm, using an XYZ-axes rotary stage (HPS80-50X-M5, Sigma Koki Co., Tokyo, Japan), which was controlled using Lab VIEW (National Instruments Co., TX, USA). Data acquisition took about 12 min. Each projection data set was then transformed into 64 bins by linear interpolation. Both the inhomogeneous sensitivity of the receiving coil and feed through interference were corrected using the method described in [23]. Transverse images were reconstructed from the projection data using the ML-EM algorithm over 15 iterations, in which the initial concentration of MNPs was assumed to be uniform [16,17].

System for MH: The details of our apparatus for MH are described in our previous papers [21,24]. In brief, an AMF was generated with use of an external coil comprising 19-turned loops (6.5 cm in diameter and 10 cm in length) of copper pipe (5 mm in diameter). This was cooled by water to ensure a constant temperature and impedance. The coil was connected to a power supply (T162-5723BHE, Thamway Co., Shizuoka, Japan) through an impedance tuner (T020-5723AHE, Thamway Co., Shizuoka, Japan). This system induced an AMF with maximum peak amplitude of 3.7 kA/m at an output power of 500 W. The amplitude of the AMF can be controlled by changing the output of the power supply. In this study, the frequency and peak amplitude of the AMF were taken as 600 kHz and 3.5 kA/m, respectively.

Preparation of TSLs encapsulating MNPs and calcein: First, 20 mg of the lipid mixture composed of DPPC and Brij78® at a molar ratio of 96:4 was dissolved in ethanol at room temperature. The solvent was removed by a rotating evaporator until a thin film formed in a round-bottom flask, after which it was dried for 24 h. The thin film was hydrated at 65°C with a PBS solution of M-300 with iron concentrations ranging from 43.8 mg/mL to 70.2 mg/mL and calcein solution (10 mM). The solution was sonicated for 5 min, and the sonication was repeated four times at an interval of 1 min. To remove the unencapsulated calcein, dialysis was carried out seven times against isotonic NaCl solution for 2 h. The unencapsulated MNPs were removed by washing with PBS and filtration through a 0.1 μm Amicon low-binding Durapore® PVDF membrane (Ultrafree, Millipore Co., MA, USA) using centrifugation at 2000 rpm for 15 min. These procedures were repeated three times. Finally, the aqueous solutions above and below the filter were collected. We refer to the TSLs encapsulating MNPs as "magnetic TSLs". We also refer to the aqueous solutions above and below the filter as "calcein-loaded magnetic TSL solution" and "aqueous solution outside the TSLs", respectively.

MPI of TSLs encapsulating MNPs and calcein: The calcein-loaded magnetic TSL solution and the aqueous solution outside the TSLs described above were put into separate cylindrical polyethylene tubes (6 mm in diameter, 5 mm in length, and 100 μL in volume) and were imaged using our MPI scanner as described above. After the MPI studies, we drew a circular region of interest (ROI) with the same area as the cross-sectional area of the polyethylene tube (115 pixels) on the MPI image and calculated the average MPI value within the ROI. In this study, the MPI value was defined as the pixel value of the transverse image reconstructed from the third-harmonic signals [16,17].

Measurement of net iron concentration in magnetic TSLs: The net iron concentration in the magnetic TSLs was determined using the potassium thiocyanate method according to the procedure published by Frascione et al. [25]. First, aliquots of 20 μL of the liposome solution were mixed with 5 μL of 1% Triton X-100 to break the liposomal membrane and to release the MNPs. Concentrated HCl (37%) with a volume of 0.225 mL was then added to the samples to ionize the iron oxide crystal core and to liberate the iron in its ferric state. The samples were incubated for a few minutes with 0.250 mL of a 40 mM potassium thiocyanate solution. The absorbance at a wavelength of 480 nm was read using a microplate absorbance spectrophotometer (xMark™, Bio-Rad Laboratories Inc., CA, USA). An aqueous solution of Fe_3O_4 was used to record calibration curve.

Measurement of temperature rise and calcein release induced by MH: We also heated the calcein-loaded magnetic TSL solution (1 mL in total volume) for 30 min using our system for MH [21,24] at an AMF frequency of 600 kHz and a peak amplitude of 3.5 kA/m, and measured the time course of the temperature rise ($\Delta T(t)$) using a fluorescence-type optical-fiber thermometer (FL-2000, Anritsu Meter Co., Tokyo, Japan) every 1 min for 30 min after the start of MH. Then, $\Delta T(t)$ was fitted to the phenomenological Box-Lucas equation given by Equation 3 [26],

$$\Delta T(t) = T(t) - T(0) = A \times (1 - e^{-Bt}) \quad \text{..... (3)}$$

Where T(t) and T(0) are the temperatures at time t and 0, respectively, and A and B are constants. This equation is often used to describe the heating of MNPs using an AMF [16]. The product of the fitting parameters, A × B, is equivalent to the initial slope of the time-dependent temperature rise $(\Delta T/\Delta t)_0$, i.e., Equation 4

$$(\Delta T/\Delta t)_0 = A \times B \quad \text{..... (4)}$$

We investigated the correlations of the average MPI value, the temperature rise, and $(\Delta T/\Delta t)_0$ with the net iron concentration of the calcein-loaded magnetic TSLs.

After heating the calcein-loaded magnetic TSL solution, we measured the calcein release using the dialysis method instead of using the self-quenching phenomenon and gel chromatography. For the measurement, the solution was dialyzed against isotonic NaCl solution for 2 h. A sample of the dialysis external solution was placed in a 96-well plate and the fluorescence intensity was measured using a plate reader at an excitation wavelength of 485 nm and an emission wavelength of 520 nm. To measure the maximum release of calcein, the sample was incubated at 50°C for 20 min using a block incubator (BI-516S, ASTEC Co., Ltd., Fukuoka, Japan). Note that the incubation temperature of 50°C was determined from the results of the calcein release measurement. The percentage of the calcein release from the calcein-loaded magnetic TSLs was calculated from Equation 5

$$\text{Release}\,(\%) = \frac{F_{AMF} - F_b}{F_{50} - F_b} \times 100 \quad \text{..... (5)}$$

Where F_b and F_{AMF} denote the fluorescence intensities of the TSL solution without and with exposure to AMF, respectively, and F_{50} is the fluorescence intensity of the sample incubated at 50°C for 20 min. The relationships between the temperature rise and calcein release and between the average MPI value and calcein release were fitted using a sigmoid function as previously described.

Animal experiments

Preparation of TSLs loading MNPs and DOX: The DOX-loaded magnetic TSLs were prepared according to the procedure described previously with some minor modifications [6,7]. After the thin film of the lipid mixture composed of DPPC and Brij78® was prepared, it was hydrated at 65°C by adding 280 mM ammonium sulphate (pH 4-4.5) and M-300 with an iron concentration of 70.2 mg/mL. After the suspension was sonicated and cooled to room temperature, DOX was encapsulated into the suspension by the pH gradient method [6,7] as previously described. In this case, the suspension and DOX were mixed at a DOX to lipid ratio of 0.2 (w/w). To remove the unencapsulated DOX, the solution was dialyzed against isotonic NaCl solution for 2 h. The unencapsulated MNPs were removed by washing with PBS and filtration through a 0.1 μm Amicon low-binding Durapore® PVDF membrane (Ultrafree, Millipore Co., MA, USA) using centrifugation at 2000 rpm for 15 min. These procedures were repeated three times.

Animals: All animal experiments were approved by the animal ethics committee at the Osaka University School of Medicine. Seven-week-old male BALB/c mice were purchased from Charles River Laboratories Japan, Inc. (Kanagawa, Japan), and were habituated to the rearing environment for one week before the experiment. The animals had free access to food and water, and were kept under standard laboratory conditions of 22-23°C room temperature, around 50% humidity, and a 12:12 hour light/dark cycle. After one-week habituation, Colon-26 cells (1×10^6 cells) were implanted subcutaneously into the back of each mouse under anesthesia by pentobarbital sodium (Somnopentyl, Kyoritsu Seiyaku Co., Tokyo, Japan) (0.012 mL/g body weight).

Tumor volumes in all mice were measured with a caliper every day. The tumor volume (V in mm^3) was calculated as Equation 6.

$$V = (\pi / 6) \times L_x \times L_y \times L_z \quad \text{.....(6)}$$

Where L_x, L_y, and L_z denote the vertical diameter, the horizontal diameter, and the height in mm, respectively. The relative tumor volume growth (RTVG) was calculated by Equation 7.

$$RTVG = \frac{V - V_0}{V_0} \quad \text{.....(7)}$$

Where V_0 represents the tumor volume immediately before MH. In this study, the RTVG value after MH was used as an index of the therapeutic effect of MH.

Experimental procedure

When the tumor volume reached approximately 100 mm^3, mice were divided into 4 groups (A, B, C, and D).The mice in Group A were injected with saline directly into the tumor as a control (n=10); the mice in Group B were injected with DOX-loaded magnetic TSLs directly into the tumor and did not undergo MH (n=7); the mice in Group C were injected with magnetic TSLs directly into the tumor and then underwent MH (n=7); and the mice in Group D were injected with DOX-loaded magnetic TSLs directly into the tumor and then underwent MH (n=7). In Groups B and D, the DOX-loaded magnetic TSLs were injected at a dose of 5 mg DOX/kg directly into the tumor under anesthesia. Ten minutes after the injection of the DOX-loaded magnetic TSLs, MPI images were obtained in the same manner as in the phantom experiments. In this study, one slice of the MPI image with the maximum signal intensity was obtained per mouse. After the MPI studies, X-ray CT images were obtained using a 4-row multi-slice CT scanner (Asteion, Toshiba Medical Systems Co., Tochigi, Japan) with a tube voltage of 120 kV and a tube current of 210 mA. The MPI image was co-registered with the X-ray CT image using parameters for magnification and rotation that were previously obtained using a phantom with 3 point sources of diameter 0.5 mm and filled with 100 mM Fe MNPs. In Groups C and D, thirty minutes after the injection of magnetic TSLs or DOX-loaded magnetic TSLs, MH was performed by applying an AMF at 600 kHz and 3.5 kA/m for 20 min. The temperature at the surface of the tumor was measured using an infrared thermometer (FLIR E4, FLIR Systems Inc., OR, USA) immediately before and after MH.

Statistical analysis

In phantom experiments, we calculated the average MPI value within a region of interest (ROI) with a diameter of 6 mm, drawn on the MPI image. The correlations of the net iron concentration in the magnetic TSLs with the average MPI value, temperature rise, and $(\Delta T/\Delta t)_0$ were analyzed using linear regression analysis and the correlation coefficients and regression equations were calculated. The correlation between the average MPI value and $(\Delta T/\Delta t)_0$ was also analyzed using linear regression analysis, whereas the correlation between the average MPI value and the temperature rise was analyzed using the phenomenological Box-Lucas equation [26] described previously.

In animal experiments, we calculated the average MPI value within the ROI drawn on the tumor by taking the threshold value for extracting the contour of the tumor as 40% of the maximum MPI value in the ROI. The correlation between the average MPI value and the temperature rise was analyzed using the phenomenological Box-Lucas equation [26] as in the phantom experiments.

Unless specifically stated, the average MPI value, temperature rise, tumor volume, and RTVG value were expressed as the mean ± standard error (SE). For comparison of the RTVG value among groups, one-way analysis of variance (ANOVA) was used. Statistical significance was determined by the Tukey-Kramer multiple comparisons test. A P value less than 0.05 was considered statistically significant. All analyses were performed using Excel 2010 (Microsoft Co., WA, USA).

Results

Temperature-dependent release of calcein and DOX from TSLs

To investigate the thermo sensitivity of TSLs, the temperature-dependent calcein and DOX releases from the TSLs were measured after 20 min of incubation. Figure 1a shows the relationship between the temperature and the percentage of calcein release from TSLs calculated from Equation (1), whereas Figure 1b shows the case of DOX. The calcein release from the TSLs steeply increased at about 38-40°C and plateaued thereafter, whereas it was almost zero at 27-36°C (Figure 1a). The temperature dependency of the DOX release was similar to that of the calcein release (Figure 1b).

Phantom experiments

Figure 2a illustrates a phantom having two cylindrical polyethylene tubes (6 mm in diameter, 5 mm in length, and 100 μL in volume) filled with aqueous solution outside TSLs (left) and the TSL solution including MNPs and calcein (right). Figures 2b-2f show examples of the MPI images of the phantom when the net iron concentration determined by the potassium thiocyanate method in the calcein-loaded magnetic TSLs was 3.9 mg/mL (b), 5.8 mg/mL (c), 6.8 mg/mL (d), 9.5 mg/mL (e), and

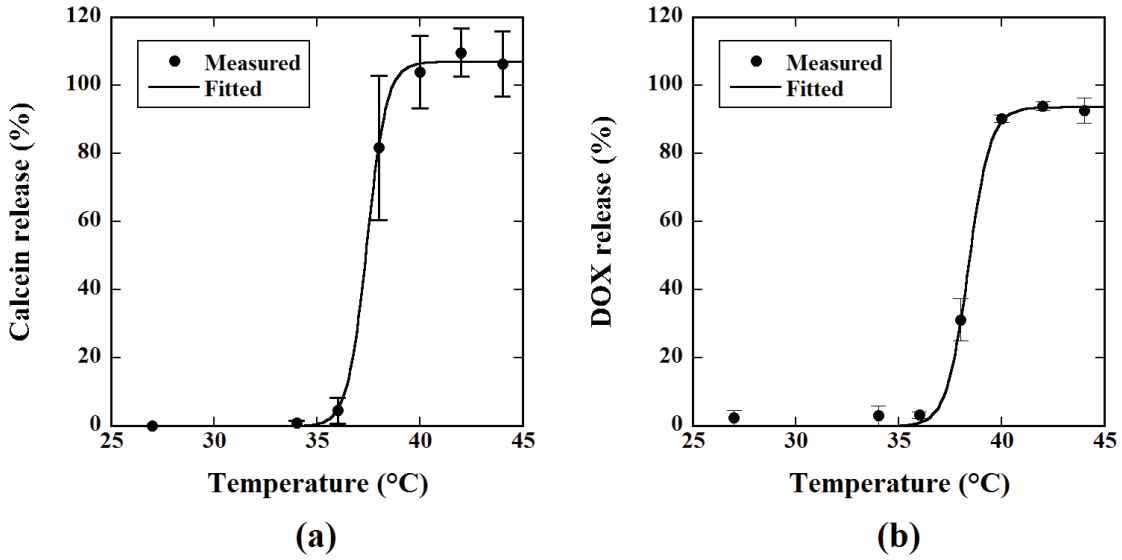

Figure 1: (a) Relationship between temperature and the percentage of the calcein release from thermosensitive liposomes (TSLs) calculated from Equation 1. **(b)** Relationship between temperature and the percentage of the doxorubicin (DOX) release from TSLs calculated from Equation 1. Data are represented by mean ± standard error (SE) for n=3.

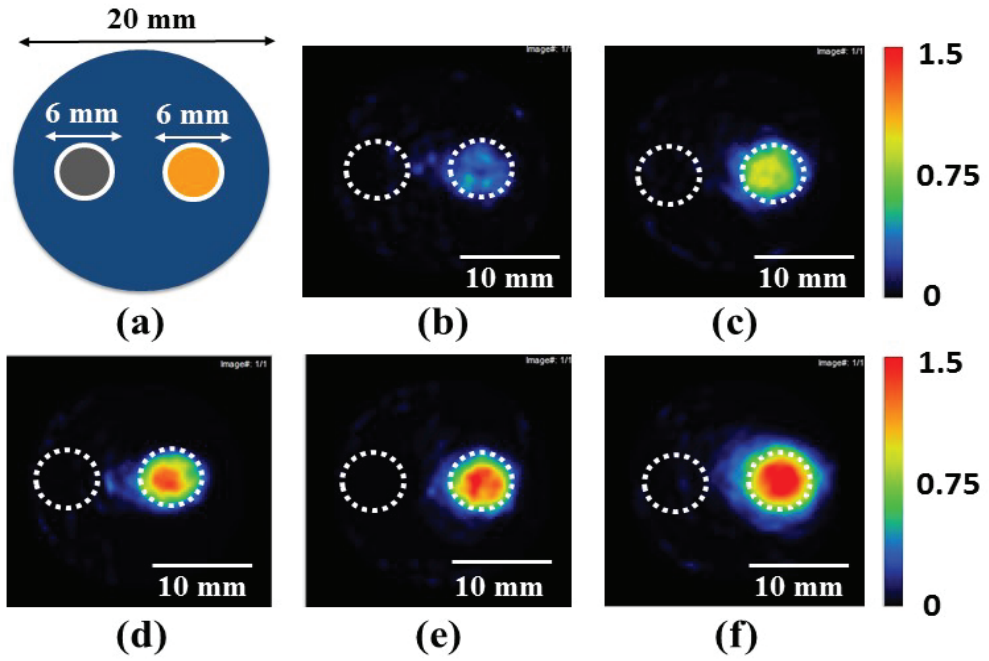

Figure 2: Illustration of a phantom having two cylindrical polyethylene tubes (6 mm in diameter, 5 mm in length, and 100 μL in volume) filled with the aqueous solutions below (aqueous solution outside the TSLs) (left) and above the filter used for removing the unencapsulated MNPs (calcein-loaded magnetic TSL solution) (right) **(a)** and examples of MPI images of the phantom when the net iron concentration determined by the potassium thiocyanate method in the magnetic TSLs was 3.9 mg/mL **(b)**, 5.8 mg/mL **(c)**, 6.8 mg/mL **(d)**, 9.5 mg/mL **(e)**, and 12.0 mg/mL **(f)**.

Note: The dotted circles in **(b)-(f)** illustrate the polyethylene tubes. Scale bar =10 mm.

12.0 mg/mL (f), respectively. As shown in Figure 2, the MPI pixel value in the left tube was almost zero in all cases, whereas that in the right tube increased with increasing iron concentration.

Figure 3 shows the time courses of the temperature rise in the calcein-loaded magnetic TSL solution, measured by a fluorescence-type optical-fiber thermometer. The symbols ○, ●, Δ, ▲, and □ show cases when the net iron concentration in the magnetic TSLs was 3.4 ± 1.0 mg/mL (mean ± standard deviation (SD) for n=4), 4.8 ± 2.8 mg/mL, 7.5 ± 3.1 mg/mL, 8.9 ± 1.8 mg/mL, and 11.5 ± 1.6 mg/mL, respectively. As shown in Figure 3, the temperature rise increased with increasing iron concentration.

Figures 4a-4c show the relationships between the net iron concentration in the calcein-loaded magnetic TSLs and the average MPI value, between the net iron concentration and the temperature rise, and between the net iron concentration and $(\Delta T/\Delta t)_0$, respectively. As shown in Figure 4, there were significant correlations in all cases and the correlation coefficient between the net iron concentration and $(\Delta T/\Delta t)_0$ was the highest (r=0.944).

Figure 5a shows the relationship between the average MPI value and the temperature rise, whereas Figure 5b shows that between the average MPI value and $(\Delta T/\Delta t)_0$. It should be noted that when analyzing the correlation between the average MPI value and the temperature rise, the phenomenological Box-Lucas equation [26] described previously was used, whereas the correlation between the average MPI value and $(\Delta T/\Delta t)_0$ was analyzed using a linear regression equation. As shown in Figure 5, the average MPI value showed significant correlations with the temperature rise (r=0.915) and $(\Delta T/\Delta t)_0$ (r = 0.923).

Figure 6a shows the relationship between the temperature rise and the percentage of calcein release from the calcein-loaded magnetic TSLs calculated from Equation 5, whereas Figure 6b shows that between the average MPI value and the percentage of calcein release. The calcein

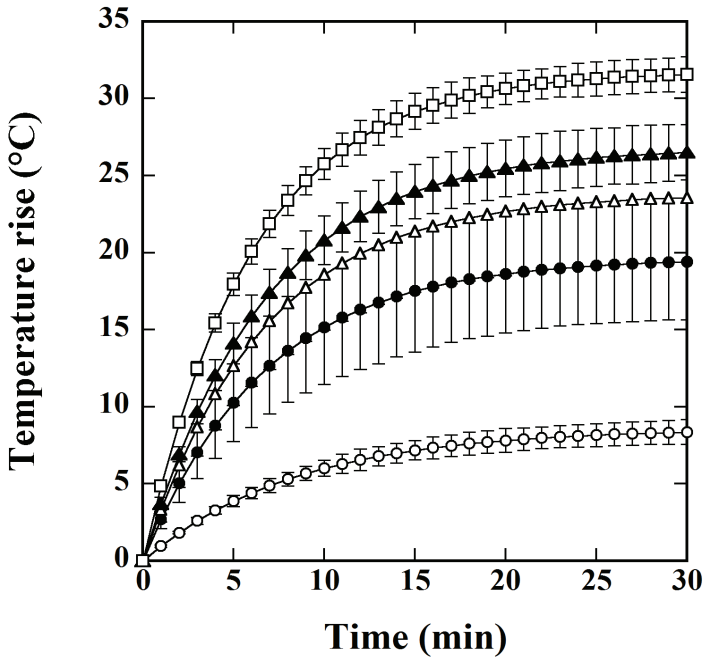

Figure 3: Time courses of the temperature rise in magnetic TSLs solution, measured by a fluorescence-type optical-fiber thermometer. The symbols ○, ●, Δ, ▲, and □ show cases when the net iron concentration in the magnetic TSLs was 3.4 ± 1.0 mg/mL (mean ± standard deviation for n=4), 4.8 ± 2.8 mg/mL, 7.5 ± 3.1 mg/mL, 8.9 ± 1.8 mg/mL, and 11.5 ± 1.6 mg/mL, respectively. Data are represented by mean ± SE for n=4.

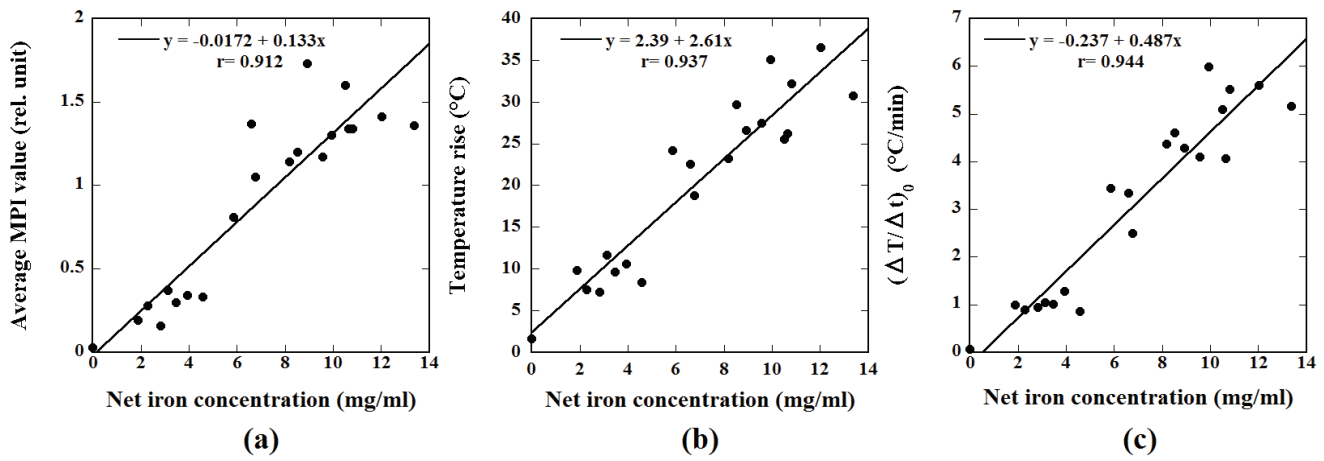

Figure 4: (a) Relationship between the net iron concentration in the magnetic TSLs and the average MPI value. **(b)** Relationship between the net iron concentration in the magnetic TSLs and the temperature rise. **(c)** Relationship between the net iron concentration in the magnetic TSLs and the initial slope of the time-dependent temperature rise $(\Delta T/\Delta t)_0$.

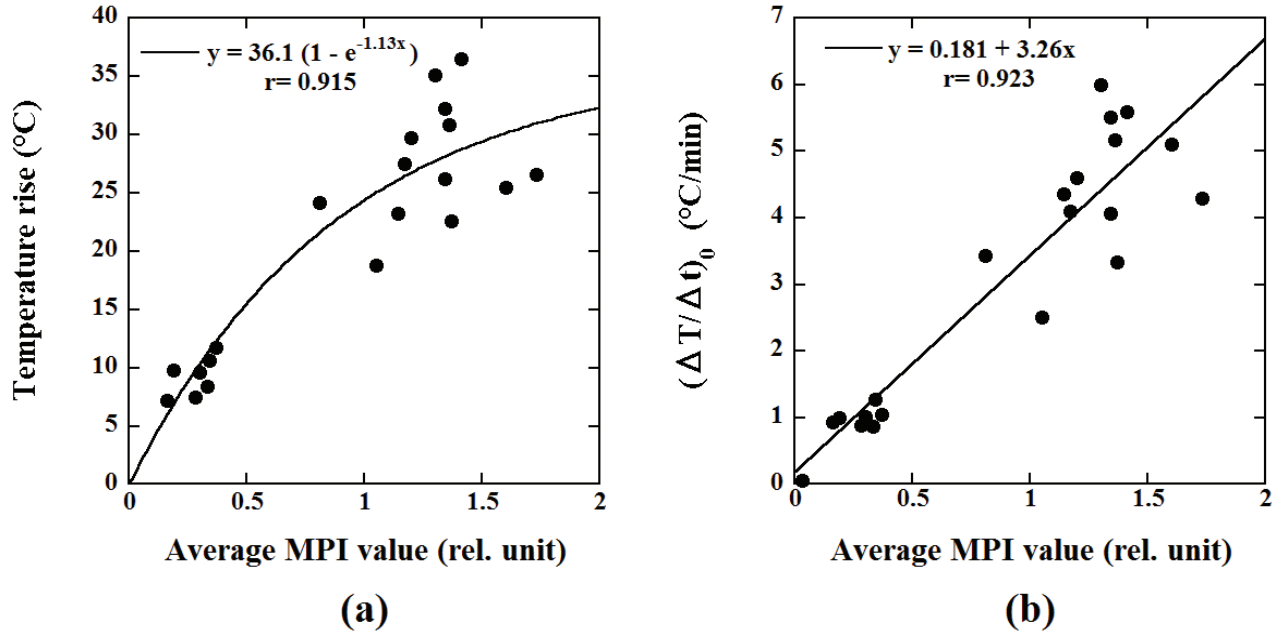

Figure 5: (a) Relationship between the average MPI value and the temperature rise. **(b)** Relationship between the average MPI value and $(\Delta T/\Delta t)_0$.

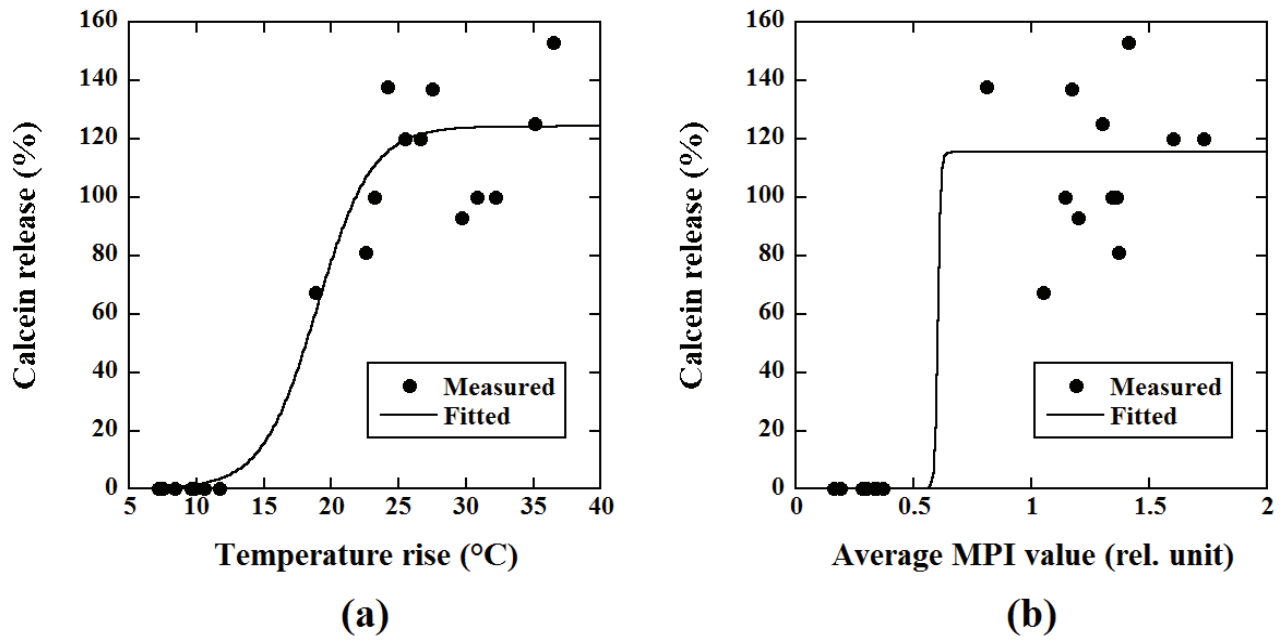

Figure 6: (a) Relationship between the temperature rise and the percentage of calcein release from the magnetic TSLs. **(b)** Relationship between the average MPI value and calcein release.

Note that the solid line represents the fitted curve using a sigmoid function.

release from the calcein-loaded magnetic TSLs fitted well to a sigmoid function and changed steeply with increasing temperature rise and average MPI value.

Animal Experiments

Figure 7 shows typical examples of MPI images of tumor-bearing mice injected with the DOX-loaded magnetic TSLs with an iron concentration of 12.0 mg/mL and a volume of 500 μL, which was superimposed on the X-ray CT image. As shown in Figure 7, the distribution of MNPs obtained by MPI correlated well with that of the tumor in the X-ray CT image in both cases.

Figures 8a and 8b show the thermal images of a tumor-bearing mouse injected with the DOX-loaded magnetic TSLs obtained by an infrared thermometer immediately before and 20 min after the start of MH, respectively. The temperature at the surface of the tumor increased from 30.9 ± 2.8 to 41.6 ± 3.4°C (mean ± SD) 20 min after the start of MH, whereas that of other regions did not rise significantly. The highest

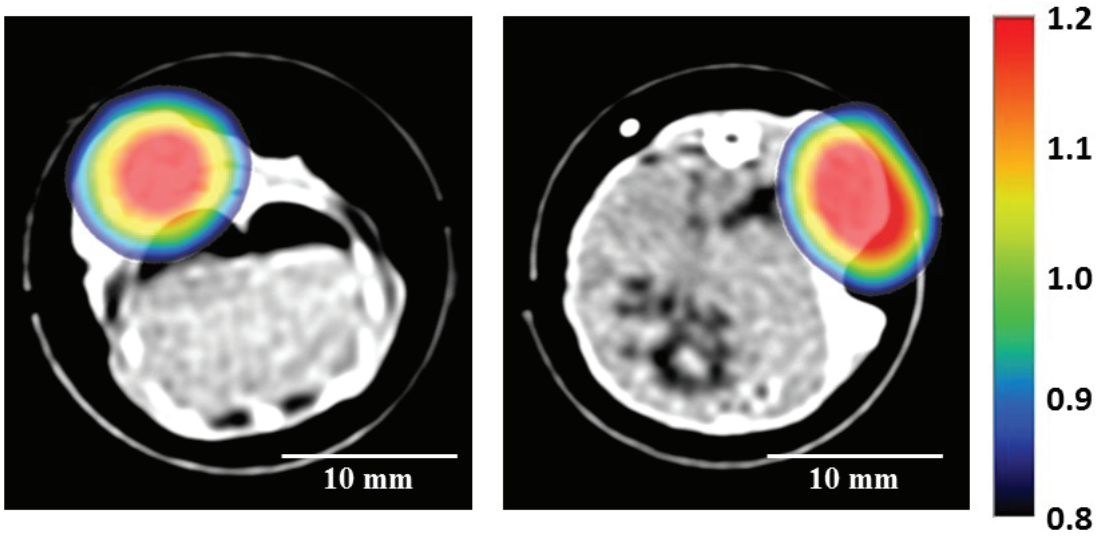

Figure 7: Typical example of MPI images of the tumor-bearing mice injected with DOX-loaded magnetic TSLs with an iron concentration of 12.0 mg/mL and a volume of 500 μL, which was superimposed on the X-ray CT image. Scale bar=10 mm.

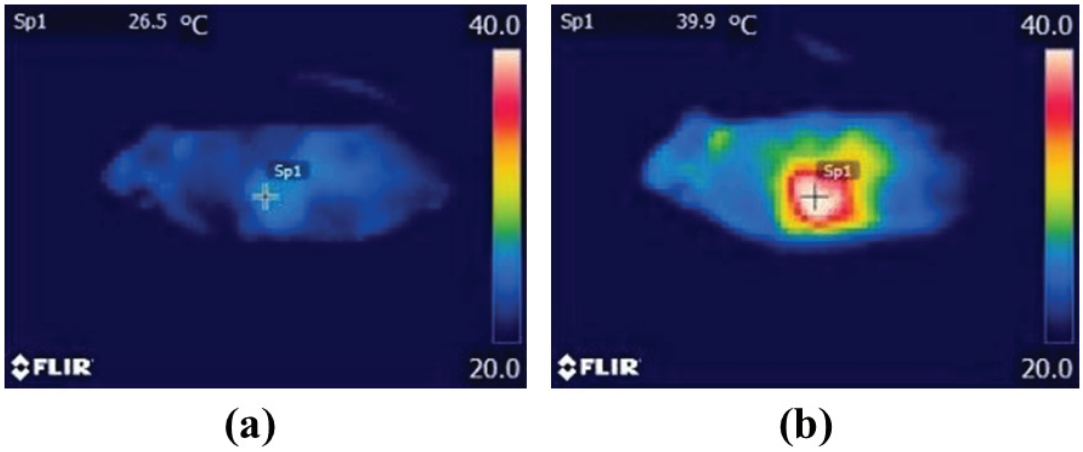

Figure 8: Thermal images of a tumor-bearing mouse injected with DOX-loaded magnetic TSLs obtained by an infrared thermometer immediately before **(a)** and 20 min after the start of MH **(b)**. Note that the lowest and highest levels for display were set at 20°C and 40°C, respectively.

temperature ranged from approximately 38 to 47°C and it lasted for at least approximately 10 min.

Figure 9 shows the relationship between the average MPI value and the temperature rise at the surface of the tumor injected with the DOX-loaded magnetic TSLs (●) and the magnetic TSLs without DOX (○) measured by an infrared thermometer 20 min after the start of MH. There was a significant correlation between them when performing regression analysis using the phenomenological Box-Lucas equation [26] (r=0.690).

Figure 10 shows the time courses of the RTVG value in Groups A (□), B (○), C (■), and D (●). There were significant differences between Groups A and B 2 to 5 days after the injection of agents. There were also significant differences between Groups A and C 3 days and 5 to 7 days after the injection of agents. There were significant differences between Groups A and D and between Groups C and D 1 day or more after the injection of agents. There were no significant differences between Groups B and C throughout the study period. There were significant differences between Groups B and D 2 to 9 days and 11 days or more after the injection of agents.

Discussion

In the present study, we developed calcein- and DOX-loaded magnetic TSLs and investigated the feasibility of visualizing them using MPI *in vitro* and *in vivo* and the therapeutic effect of chemotherapy using the DOX release induced by MH *in vivo*. Our results (Figures 1-10) demonstrated that our magnetic TSLs can be applied to MPI and MH as nanocarriers. Liposomes have the remarkable ability to carry drugs to a desired targeted site and of reducing drug toxicity by encapsulating the drugs. TSLs are one of the most attractive nanocarriers for cancer therapy when combined with local hyperthermia, because they can release encapsulated drugs under the hyperthermic condition (40-42°C) through the disruption of liposomal membranes by moderately elevating the temperature [1,6]. For this reason, many attempts to combine TSLs and local hyperthermia have been

conducted and their effectiveness has been studied using tumor-bearing mice [27,28]. Some clinical trials have also been performed using TSLs comprising DPPC and DOX (ThermoDox®, Celsion Co., NJ, USA) [29,30].

MNPs can be used as a heating source upon stimulation by AMF. Tai et al. [31] developed magnetic TSLs encapsulating dextran-coated iron oxide nanoparticles (Resovist®) and carboxylfluorescein, and demonstrated the drug release induced by MH [31]. Although they used Resovist® as a source of MNPs, we used magnetic fluid (M-300) in this study due to its availability. MNPs can be used as contrast agents for MRI and thus the liposomes encapsulating MNPs can be visualized using MRI [13]. When using a conventional T2*-weighted imaging sequence, however, the image contrast decreases (negative contrast) due to a susceptibility-induced MR signal loss. Currently, MPI has gained much attention as another imaging method for MNPs. MPI can image the spatial distribution of MNPs in positive contrast [20-22]. If we could develop TSLs encapsulating both MNPs and anticancer drugs, we may expect that diagnosis using MPI and therapy using the drug release induced by MH can be integrated.

As shown in Figure 1a, the calcein release from our calcein-loaded TSLs after 20 min incubation steeply increased at about 38-40°C and plateaued thereafter, whereas there was no significant release at around body temperature (36°C). Our calcein-loaded TSLs eventually released approximately 100% calcein at 42°C. Tagami et al. [6,7] have developed HaT-liposomes composed of DPPC and Brij78® at a molar ratio of 96:4. The HaT-liposomes have an optimum formulation for contrast-enhanced MRI using Gd-DTPA and for drug release accompanied by hyperthermia. Tagami et al. [6,7] reported that the HaT-liposomes showed more drug release at 40-42°C than the low temperature-sensitive liposome (LTSL) formulation, and showed blood pharmacokinetics similar to that of the LTSL formulation. As shown in Figure 1b, our DOX-loaded TSLs exhibited approximately 100% DOX release at 42°C after 20 min incubation and no significant DOX release at lower temperature (27-36°C). This temperature-dependent DOX release from our DOX-loaded TSLs was similar to that of the calcein release from our calcein-loaded TSLs (Figure 1a). As previously described, DOX was encapsulated into the TSLs using the pH gradient method [6,7] in this study. The above findings suggest that the pH gradient method is effective for encapsulating DOX into the TSLs.

The magnetic TSLs developed in this study could be successfully visualized by our MPI scanner in positive contrast (Figure 2). To the best of our knowledge, this is the first report to show that magnetic TSLs can be visualized using MPI. We previously reported that the average MPI value has an excellent linear correlation with the iron concentration of MNPs [20]. Therefore, the fact that the MPI value of the left tube in the phantom shown in Figure 2 was much lower than that of the right tube appears to demonstrate that almost all the unencapsulated MNPs were removed by repeated washing with PBS and filtration using centrifugation.

We could observe the temperature rise induced by MH in our magnetic TSLs both *in vitro* (Figure 3) and *in vivo* (Figure 8). Furthermore, the temperature rise became higher with increasing iron concentration (Figure 4), indicating that MNPs were successfully encapsulated into the TSLs in a concentration-dependent manner. As previously described, we quantified the net iron concentration in the magnetic TSLs using the potassium thiocyanate method and the net iron concentration thus obtained had significant correlations with the average MPI value (r=0.912), the temperature rise (r=0.937), and $(\Delta T/\Delta t)_0$ (r=0.944) (Figure 4). Note that $(\Delta T/\Delta t)_0$ was obtained by fitting the time course of the temperature rise (Figure 3) to the phenomenological Box-Lucas equation [26]. As shown in Figure 5, the average MPI value also had significant correlations with the temperature rise (r=0.915) and $(\Delta T/\Delta t)_0$ (r=0.923). These results suggest that it is possible to control the temperature rise induced by MH by changing the iron concentration of MNPs encapsulated in the magnetic TSLs, which will be useful for reducing the side effects and unwanted damage to surrounding healthy tissues in MH. These results also suggest that our MPI scanner can estimate the iron concentration in the magnetic TSLs using the average MPI value and predict the temperature rise that will be induced by MH.

As previously described, when measuring the calcein release from our magnetic TSLs in phantom experiments, the unencapsulated calcein and unencapsulated MNPs were removed by repetitive dialysis and by repetitive washing with PBS and filtration using centrifugation, respectively, instead of using gel chromatography. This is mainly because if we used gel chromatography for removing the unencapsulated calcein and MNPs, the concentration of the magnetic TSLs was considerably diluted and thus our MPI scanner could not detect the magnetic TSLs. As shown in Figure 6a, the relationship between the calcein release induced by MH and the temperature rise fitted well to a sigmoid function, as in Figure 1a. Although the relationship between the calcein release and the average MPI value also fitted a sigmoid function, the scatter of the data was large (Figure 6b). This large scattering of the data may be due to the fact that the reproducibility of the above repetitive dialysis and/or washing and filtration is low. As shown in Figure 6b, the calcein release induced by MH increased steeply like a step function with increasing average MPI value, suggesting that the average MPI value can be used to predict the threshold in drug release from the magnetic TSLs induced by MH.

Finally, we performed animal experiments to investigate the feasibility of the practical application of our magnetic TSLs. We prepared tumor-bearing mice by inoculating murine Colon-26 cells subcutaneously into the backs of mice. As shown in Figure 7, our MPI scanner could visualize the spatial distribution of the DOX-loaded magnetic TSLs in the tumor in positive contrast. This excellent visibility of MPI will be useful for the diagnosis of cancer. When combined with MPI, our DOX-loaded magnetic TSLs will also provide useful information about the location of the tumors. As shown in Figure 9, the average MPI value had a significant correlation with the temperature rise (r=0.690) when analyzed using the phenomenological Box-Lucas equation [26], suggesting that our MPI scanner can predict the temperature rise in the tumor induced by MH. This will be useful for monitoring and predicting the therapeutic response to chemotherapy using the drug release induced by MH.

When the DOX-loaded magnetic TSLs were injected into the tumor and MH was applied (Group D), the RTVG value was significantly lower than that in the case when saline was injected into the tumor and MH was not applied (Group A) (Figure 10), indicating that the combination of our DOX-loaded magnetic TSLs and MH is useful for cancer therapy. The RTVG value in Group D was also significantly lower than that in the case when the DOX-loaded magnetic TSLs were injected and MH was not applied (Group B) 2 to 9 days and 11 days or more after the injection of the DOX-loaded magnetic TSLs. This result appears to indicate the therapeutic effect of the DOX released from the DOX-loaded magnetic TSLs induced by MH. However, there was a tendency for the RTVG value in group B to be lower than that in Group A (there were significant differences between them 2 to 5 days after the injection of the DOX-loaded magnetic TSLs or saline). This may be due to the fact that there was some leakage of DOX from the DOX-loaded TSLs at body temperature. As previously described, the molar ratio of DPPC and Brij78® for preparing the TSLs was taken to be 96:4 in this study. It would be possible to reduce the above leakage by changing the molar ratio of DPPC and Brij78®. These studies are currently in progress.

A limitation of this study is that the DOX-loaded magnetic TSLs were injected directly into the tumor in order to accumulate as many MNPs and DOX in tumors as possible. If the DOX-loaded magnetic TSLs were adsorbed only to tumors, they could be administered intravenously. This

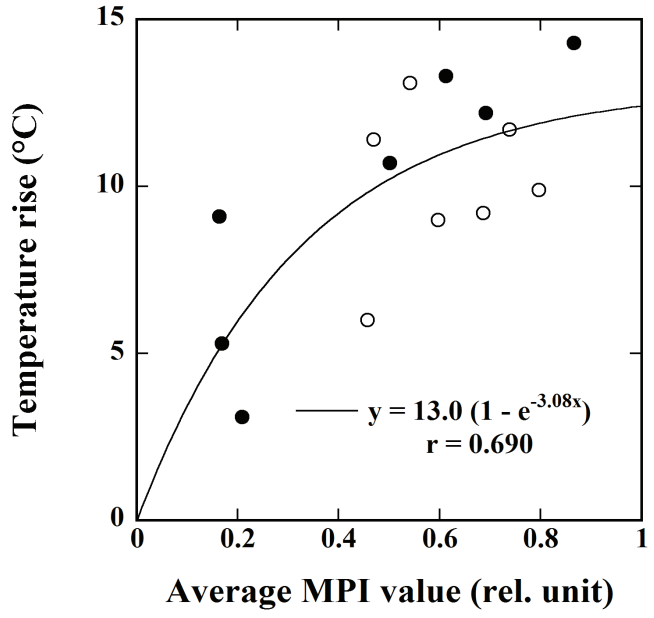

Figure 9: Relationship between the average MPI value and the temperature rise at the surface of the tumor injected with the DOX-loaded magnetic TSLs (●) and the magnetic TSLs (○) measured by an infrared thermometer 20 min after the start of MH.

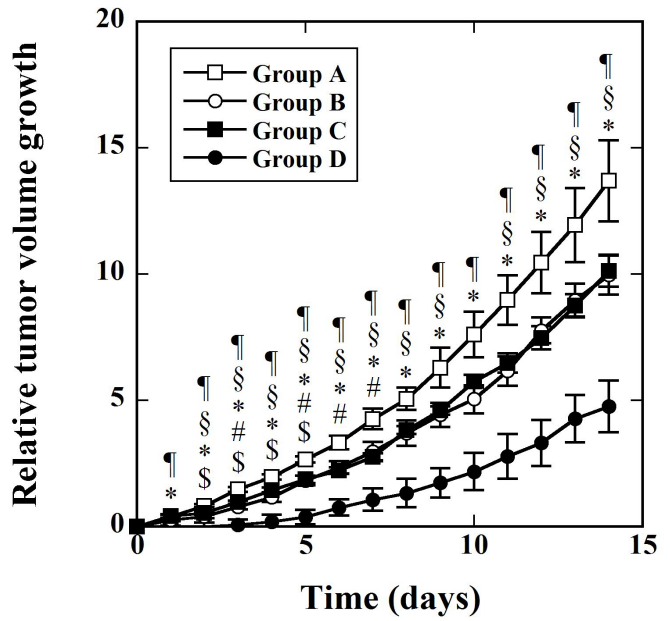

Figure 10: Time courses of the relative tumor volume growth (RTVG) in Groups A, B, C, and D. RTVG is defined as $(V-V_0)/V_0$ with V_0 and V being the tumor volumes immediately before and after injection of agents, respectively. The mice in Group A (□) were injected with saline directly into the tumor as controls (n=10); the mice in Group B (○) were injected with DOX-loaded magnetic TSLs directly into the tumor and did not undergo MH (n=7); the mice in Group C (■) were injected with magnetic TSLs directly into the tumor and then underwent MH (n=7); and the mice in Group D (●) were injected with DOX-loaded magnetic TSLs directly into the tumor and then underwent MH (n=7). Data are represented by mean ± SE. $: p<0.05 between Groups A and B, #: p<0.05 between Groups A and C, *: p<0.05 between Groups A and D, §: p<0.05 between Groups B and D, and ¶ : p<0.05 between Groups C and D.

feature will be highly important when considering practical applications. However, because the administered magnetic TSLs migrate passively to mononuclear phagocyte systems such as the Kupffer cells of the liver and spleen, passive targeting is a very important issue for the establishment of cancer therapy. Shido et al. [32] and Motoyama et al. [33] have developed magnetite cationic liposomes (MCLs) for improving absorption and accumulation properties within tumors, because MCLs have a positive electric charge at the liposomal surface. Administration of the MCLs, however, is limited to direct injection into the tumor at present [34]. The conjugation of antibodies to liposomal membranes may be a possible approach for active targeting of tumors with magnetic TSLs. Thus, we will develop antibody-conjugated magnetic TSLs having tumor-specific targeting ability in the future.

Conclusion

We developed the calcein- and DOX-loaded magnetic TSLs and could visualize them using MPI both *in vitro* and *in vivo*. Our results suggest that they are useful as drug delivery nanocarriers in nanomedicine. Our results also suggest that MPI is useful for enhancing the therapeutic effect of the chemotherapy using the drug release from the magnetic TSLs encapsulating anticancer drugs, because MPI can visualize the magnetic TSLs in positive contrast and allows us to quantify the iron concentration in the magnetic TSLs for predicting the drug release induced by MH.

Acknowledgements

This work was supported by a Grant-in-Aid for Scientific Research (Grant Number: 25282131) from the Japan Society for the Promotion of Science (JSPS).

Declaration of interest

The authors report no conflicts of interest.

References

1. Kneidl B, Peller M, Winter G, Lindner LH, Hossann M (2014) Thermosensitive liposomal drug delivery systems: state of the art review. Int J Nanomedicine 9: 4387-4398.
2. Akbarzadeh A, Rezaei-Sadabady R, Davaran S, Joo SW, Zarghami N, et al. (2013) Liposome: classification, preparation, and applications. Nanoscale Res Lett 8: 102.
3. Allen TM, Hansen C, Martin F, Redemann C, Yau-Young A (1991) Liposomes containing synthetic lipid derivatives of poly(ethylene glycol) show prolonged circulation half-lives *in vivo*. Biochim Biophys Acta 1066: 29-36.
4. Blume G, Cevc G (1993) Molecular mechanism of the lipid vesicle longevity *in vivo*. Biochim Biophys Acta 1146: 157-168.
5. Yatvin MB, Weinstein JN, Dennis WH, Blumenthal R (1978) Design of liposomes for enhanced local release of drugs by hyperthermia. Science 202: 1290-1293.
6. Tagami T, Ernsting MJ, Li SD (2011) Optimization of a novel and improved thermosensitive liposome formulated with DPPC and a Brij surfactant using a robust *in vitro* system. J Control Release 154: 290-297.
7. Tagami T, Foltz WD, Ernsting MJ, Lee CM, Tannock IF, et al. (2011) MRI monitoring of intratumoral drug delivery and prediction of the therapeutic effect with a multifunctional thermosensitive liposome. Biomaterials 32: 6570-6578.
8. Kobayashi T, Kakimi K, Nakayama E, Jimbow K (2014) Antitumor immunity by magnetic nanoparticle-mediated hyperthermia. Nanomedicine (Lond) 9: 1715-1726.
9. Dewhirst MW, Prosnitz L, Thrall D, Prescott D, Clegg S, et al. (1997) Hyperthermic treatment of malignant diseases: current status and a view toward the future. Semin Oncol 24: 616-625.

10. Neuberger T, Schopf B, Hofmann H, Hofmann M, Rechenberg B (2005) Superparamagnetic nanoparticles for biomedical applications: Possibilities and limitations of a new drug delivery system. J Magn Magn Mater 293: 483-496.

11. Rosensweig RE (2002) Heating magnetic fluid with alternating magnetic field. J Magn Magn Mater 252: 370-374.

12. Araya T, Kasahara K, Nishikawa S, Kimura H, Sone T, et al. (2013) Antitumor effects of inductive hyperthermia using magnetic ferucarbotran nanoparticles on human lung cancer xenografts in nude mice. Onco Targets Ther 6: 237-242.

13. Béalle G, Di Corato R, Kolosnjaj-Tabi J, Dupuis V, Clément O, et al. (2012) Ultra magnetic liposomes for MR imaging, targeting, and hyperthermia. Langmuir 28: 11834-11842.

14. Gleich B, Weizenecker J (2005) Tomographic imaging using the nonlinear response of magnetic particles. Nature 435: 1214-1217.

15. Goodwill PW, Konkle JJ, Zheng B, Saritas EU, Conolly SM (2012) Projection x-space magnetic particle imaging. IEEE Trans Med Imaging 31: 1076-1085.

16. Murase K, Hiratsuka S, Song R, Takeuchi Y (2014) Development of a system for magnetic particle imaging using neodymium magnets and gradiometer. Jpn J Appl Phys 53: 067001.

17. Murase K, Song R, Hiratsuka S (2014) Magnetic Particle Imaging of blood coagulation. Appl Phys Lett 104: 252409.

18. Pradhan P, Giri J, Rieken F, Koch C, Mykhaylyk O, et al. (2010) Targeted temperature sensitive magnetic liposomes for thermo-chemotherapy. J Control Release 142: 108-121.

19. Murata K, Kohno K (1989) Nonlinear least-squares regression analysis by a simplex method using differential equations containing Michaelis-Menten type rate constants. Biopharm Drug Dispos 10: 25-34.

20. Murase K, Aoki M, Banura N, Nishimoto K, Mimura A, et al. (2015) Usefulness of magnetic particle imaging for predicting therapeutic effect of magnetic hyperthermia. Open J Med Imaging 5: 85-99.

21. Murase K, Mimura A, Banura N, Nishimoto K, Takata H (2015) Visualization of magnetic nanofibers using magnetic particle imaging. Open J Med Imaging 5: 56-65.

22. Nishimoto K, Mimura A, Aoki M, Banura N, Murase K (2015) Application of magnetic particle imaging using nebulized magnetic nanoparticles. Open J Med Imaging 5: 49-55.

23. Murase K, Banura N, Mimura A, Nishimoto K (2015) Simple and practical method for correcting the inhomogeneous sensitivity of a receiving coil in magnetic particle imaging. Jpn J Appl Phys 54: 038001.

24. Murase K, Oonoki J, Takata H, Song R, Angraini A, et al. (2011) Simulation and experimental studies on magnetic hyperthermia with use of superparamagnetic iron oxide nanoparticles. Radiol Phys Technol 4: 194-202.

25. Frascione D, Diwoky C, Almer G, Opriessnig P, Vonach C, et al. (2012) Ultrasmall superparamagnetic iron oxide (USPIO)-based liposomes as magnetic resonance imaging probes. Int J Nanomedicine 7: 2349-2359.

26. Box GEP, Lucas HL (1959) Design of experiments in nonlinear situations. Biometrika 46: 77-90.

27. Kono K, Nakashima S, Kokuryo D, Aoki I, Shimomoto H, et al. (2011) Multi-functional liposomes having temperature-triggered release and magnetic resonance imaging for tumor-specific chemotherapy. Biomaterials 32: 1387-1395.

28. Tagami T, Ernsting MJ, Li SD (2011) Efficient tumor regression by a single and low dose treatment with a novel and enhanced formulation of thermosensitive liposomal doxorubicin. J Control Release 152: 303-309.

29. Wood BJ, Poon RT, Locklin JK, Dreher MR, Ng KK, et al. (2012) Phase I study of heat-deployed liposomal doxorubicin during radiofrequency ablation for hepatic malignancies. J Vasc Interv Radiol 23: 248-255.

30. Landon CD, Park JY, Needham D, Dewhirst MW (2011) Nanoscale drug delivery and hyperthermia: the materials design and preclinical and clinical testing of low temperature-sensitive liposomes used in combination with mild hyperthermia in the treatment of local cancer. Open Nanomed J 3: 38-64.

31. Tai LA, Tsai PJ, Wang YC, Wang YJ, Lo LW, et al. (2009) Thermosensitive liposomes entrapping iron oxide nanoparticles for controllable drug release. Nanotechnology 20: 135101.

32. Shido Y, Nishida Y, Suzuki Y, Kobayashi T, Ishiguro N (2010) Targeted hyperthermia using magnetite cationic liposomes and an alternating magnetic field in a mouse osteosarcoma model. J Bone Joint Surg Br 92: 580-585.

33. Motoyama J, Hakata T, Kato R, Yamashita N, Morino T, et al. (2008) Size dependent heat generation of magnetite nanoparticles under AC magnetic field for cancer therapy. Biomagn Res Technol 6: 4.

34. Kawai N, Ito A, Nakahara Y, Honda H, Kobayashi T, et al. (2006) Complete regression of experimental prostate cancer in nude mice by repeated hyperthermia using magnetite cationic liposomes and a newly developed solenoid containing a ferrite core. Prostate 66: 718-727.